Rubber-Modified Epoxies. IV. Influence of Morphology on Mechanical Properties

D. VERCHERE,[1] J. P. PASCAULT,[1] H. SAUTEREAU,*[1] S. M. MOSCHIAR,[2]
C. C. RICCARDI,[2] and R. J. J. WILLIAMS[2]

[1]Laboratoire des Matériaux Macromoléculaires, URA CNRS n°. 507, Institut National des Sciences Appliquées de Lyon, 20, Avenue A. Einstein, 69621 Villeurbanne Cedex, France; [2]Institute of Materials Science and Technology (INTEMA), University of Mar del Plata and National Research Council (CONICET) 7600 Mar del Plata, Argentina

SYNOPSIS

The mechanical properties of a system consisting of a bisphenol A diglycidylether (DGEBA) epoxy, cured with a cycloaliphatic diamine (4,4'-diamino-3,3 dimethyldicyclohexyl-methane, 3DCM), in the presence of an epoxy-terminated butadiene–acrylonitrile random copolymer (ETBN), was studied as a function of the cure schedule and the initial rubber concentration. Fracture toughness (K_{Ic}) and fracture energy (G_{Ic}) were increased, while Young's modulus and yield strength decreased slightly with increasing volume fraction of the dispersed phase. We show that there is no significant influence of the precure schedule and of the various observed particle diameters on the mechanical properties for a constant rubber volume fraction. In our case, the main deformation process in the rubber-modified epoxy networks is shear yielding while cavitation is negligible.

INTRODUCTION

In the context of a cooperation program between our laboratories, a particular rubber-modified epoxy was carefully studied to get a deeper understanding of the different factors affecting the phase-separation process, the resulting morphologies, and mechanical properties. The particular system consists of a bisphenol A diglycidyl ether (DGEBA)-based epoxy cured with a cycloaliphatic diamine (4,4'-diamino-3,3' dimethyldicyclohexylmethane, 3DCM), in the presence of an epoxy-terminated butadiene–acrylonitrile random copolymer (ETBN).

In the first part of this series, the influence of ETBN on the polymerization and phase-separation processes was reported.[1]

In the second part, the volume fraction of the dispersed phase, the concentration of dispersed-phase particles, and the composition of both phases at functions of polymerization temperature and rubber concentration were discussed.[2]

In the third part of this series,[3] a phase-separation model was used to simulate the morphologies obtained in the second part.[2] The model, based on a thermodynamic description through a Flory–Huggins equation, and constitutive equations for polymerization and phase-separation rates, was able to explain most of the observed trends.

The aim of this fourth part is to analyze and discuss the mechanical properties and to find correlations with the generated morphologies.

The mechanical properties of rubber-toughened epoxies depend strongly on the morphology developed during the phase-separation process, including the total rubber-content,[4–12] the volume fraction of the rubber phase,[11–14] and the rubber particle size and distribution. Other studies suggest that interparticle distance, which could alter the overlapping stress fields between particles, plays an important role.[15,16]

Bascom et al.[17] found that in rubber-modified epoxy adhesives plastic-zone size is directly related

* To whom correspondence should be addressed.

Journal of Applied Polymer Science, Vol. 43, 293–304 (1991)
 CCC 0021-8995/91/020293-12$04.00

to the toughness. They proposed that cavitation caused by the triaxial tension ahead of the crack tip increases the size of the plastic zone and that plastic flow of the epoxy matrix and elongation of the particles also contribute to the toughness. Kinloch et al.[18] and Yee and Pearson[19-21] presented TEM and SEM micrographs to support the notion that cavitation and plastic shear yielding of the epoxy matrix are the microdeformation mechanisms occurring at the crack tip that dissipate energy and produce the toughening effect. Yee and Pearson indicated that at low strain rates the rubber particles simply enhance shear deformation and at sufficiently high strain rates the rubber particles cavitate and subsequently promote further shear deformation and that no major effects due to particle-size differences had been observed. The increased size of the plastic zone at the crack tip associated with decreasing yield strength could be the cause of the increased toughness.[18-23]

EXPERIMENTAL

Materials

The DGEBA diepoxy prepolymer used was DER 332 (Dow Chemical), with an equivalent weight of epoxy groups equal to 174.3 g/eq ($\bar{n} = 0.03$). The diamine, a cycloaliphatic one, was 4,4′-diamino-3,3′ dimethyldicyclohexylmethane (3DCM, Laromin C260, BASF)·ETBN adducts with the DGEBA ($\bar{n} = 0.03$), were prepared following a procedure previously described.[7] This procedure essentially consists of an almost complete reaction of carboxyl groups with epoxy functions, using a carboxyl-to-epoxy ratio equal to 0.065 at 85°C, in the presence of 0.18% by weight of triphenylphosphine. Because of the large excess of DGEBA, most of the ETBN consists of a solution of a triblock copolymer (DGEBA/CTBN/DGEBA) in the epoxy monomer. The CTBN used is 1300 × 8 (Goodrich) with 18% of acrylonitrile.

The formulations were prepared by combining the selected amount of ETBN and the epoxy monomer, stirring under vacuum at moderate temperatures, cooling to room temperature, and mixing with a stoichiometric proportion of diamine (with respect to the sum of epoxides coming from the monomer and adduct). The rubber concentration in the formulation will be expressed as a percentage of mass fraction (% R) or as a volume fraction ϕ_R. Four different initial rubber concentrations were selected: % R = 6.5, 10.6, 15, and 20. Different precure temperatures were selected: 29, 50, 75, and 100°C (see Part II).

Crack Propagation

Crack propagation in epoxy resins is studied using a linear elastic fracture mechanics approach since epoxies are normally brittle and display approximately linear elastic deformation behavior with very little plastic deformation. Epoxy networks are prone to crack propagation by means of a continuous (stable) mode or by a crack jumping (unstable or "stick-slip") mode.[22-30] Continuous crack propagation gives rise to a smooth load-displacement curve during propagation, whereas "stick-slip" propagation leads to the characteristic "saw-tooth" curve illustrated schematically in Figure 1.

There are many factors that control the propagation of cracks and the resulting fracture surface morphology in epoxy resins[24]: (1) specimen geometry; (2) amount and type of curing agent; and (3) environment and testing rate.[22-30]

When continuous crack propagation occurs, a constant crack opening displacement at the crack

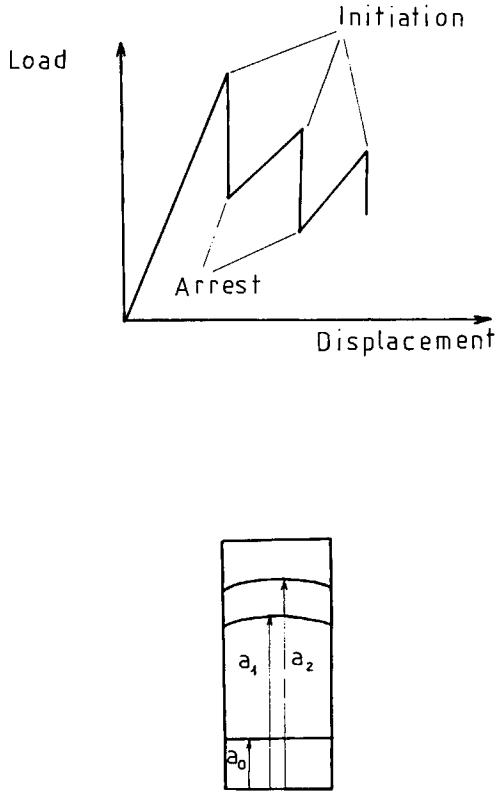

Figure 1 Typical load-displacement curves during crack propagation and fracture surface of specimen after crack propagation.

tip provides a unique failure criterion, and the value of this parameter rises rapidly when the material undergoes a transition from stable to stick-slip propagation. This was interpreted as a clear indication that blunting of the crack tip took place when stick-slip propagation resulted. The yield stresses of the epoxy materials decrease as the strain rate is reduced and the temperature is raised. This implies that plastic deformation is promoted under these conditions. These conditions are also the ones that favor stick-slip crack propagation.[23]

Single-edge-notched testing of precracked test specimens was used for determining the toughness of the epoxy systems. Initial crack lengths were between 0.5 and 2 mm in the side of the samples.

Second cracks were made with a razor blade. The cracks were introduced into the test specimens by carefully tapping a sharp blade into a narrow saw cut in the center of the specimen submitted to compressive stress. The depths of all the cracks were between 1 and 5 mm and the tip on the order of magnitude of 1 μm. The ratio a/w, crack length divided by width, varies between 0.08 and 0.42. Initial crack length was determined by observing the markings on the fracture surface with a microscope.

The minimum sample dimensions required to obtain a valid K_{Ic} measurement are determined by the size of the plastic zone and, thus, by the value of K_{Ic} and the yield stress, σ_y, of the material.[31] For the dimensions used here, the test should be valid for crack length values greater than 1 mm.

The samples (Fig. 2) were loaded to failure in a tensile machine (DY25, Adamel-Lhomargy) using a crosshead speed of 1 mm/min ($\dot{\epsilon} = 5.2 \cdot 10^{-4}\ s^{-1}$)[28] at room temperature. With these conditions and for our system, the samples are prone to crack propagation by means of a crack jumping (unstable or "stick-slip" mode[22-30]) (Fig. 1). This means that as the load reaches a critical level (P_i) the crack propagates while the load drops. When the load reaches a lower critical level (P_a), the crack stops and then the load increases again. Two stress intensity factors can thus be defined: K_{Ici} (initiation) and K_{Ica} (arrest) corresponding to P_i and P_a, respectively. The use of these two factors is helpful to characterize the slip-stick behavior. As the crack stops, a crack arrest regions forms at the tip of the crack. The crack then slowly propagates through the plastic zone. Then, the crack rapidly propagates through virgin material. The crack arrest region, readily visible on fractured surfaces, is, thus, a slow-growth region corresponding to the plastic zone at the crack tip.

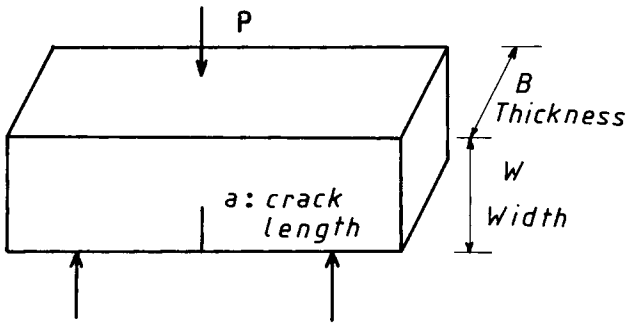

Figure 2 Specimen configuration—single-edge-notched (three-point-bending).

Analysis

Glass transition temperatures (T_g) were determined with a differential scanning calorimeter (Mettler TA300). The analyses were performed under argon atmosphere, with a heating rate of 10 K/min.

Tensile and compressive tests were performed at room temperature with a tensile testing machine (DY25, Adamel-Lhomargy). For the tensile tests, strain measurements were performed using an extensometer (EX-10) at a strain rate of $3.3 \cdot 10^{-4}\ s^{-1}$, using ISO-60 standard specimens. Samples of dimension 20 × 12 × 6 mm were deformed in a compression cage between polished steel plates. The nominal strain was determined by averaging the results from two linear variable differential transformer (LVDT) transducers. The strain rate used was $8.3 \cdot 10^{-4}\ s^{-1}$.

Fracture toughness was studied with opening mode I tests and in a plane strain state. The single-edge-notched (SEN) test specimen is shown in Figure 2.

Values of K_{Ic} are calculated by using the following formula:

$$K_{Ic} = \sigma_c \sqrt{\pi a} \cdot Y(a/w)$$

where w = specimen width; a = crack length; and σ_c = critical fracture stress.

The correction factor taken equal to $Y(a/w) = 1.09 - 1.735\ a/w + 8.2\ (a/w)^2 - 14.18\ (a/w)^3 + 14.57\ (a/w)^4$ in accordance with Ref.[31]

Once K_{Ic} is determined, G_{Ic} can be calculated by using the following relationship:

$$G_{Ic} = \frac{K_{Ic}^2}{E}(1 - \nu^2)$$

where ν = Poisson's ratio and E = Young's modulus.

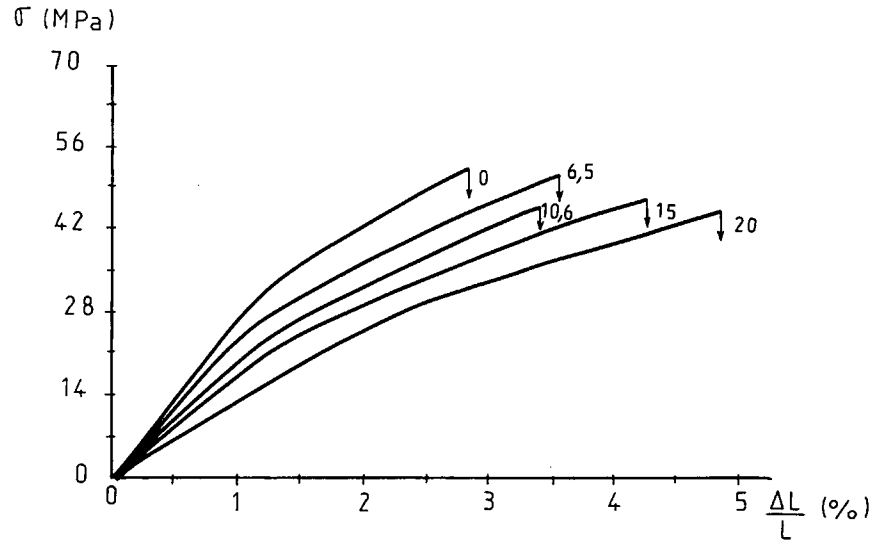

Figure 3 Influence of rubber content on the engineering tensile stress–strain curves of rubber-modified epoxies ($\dot{\epsilon} = 3 \cdot 10^{-4}$ s^{-1}) at room temperature. Systems: DGEBA ($\bar{n} = 0.03$)–3DCM–n% R8; 6.5% R8; 10.6% R8; 20% R8 precure cycle 75°C.

RESULTS AND DISCUSSION

Influence of Rubber Content on Mechanical Properties

The rubber-modified epoxy networks were achieved as described in the first part of this series. Various amounts of rubber R8 were introduced with up to 20% by weight. The precure schedules were chosen so as to modify the mean rubber particle size. The maximum glass transition temperature, ${}_E T_{g\infty}$, values, and morphology characteristics are listed in the second part.[2]

The Young's moduli are determined by using the tensile stress–strain curves shown in Figure 3 and Table I. As expected, the elastic modulus decreases

Table I Mechanical Properties at Room Temperature as Functions of Cure Schedule for Specimens with Different Percentages of Rubber

		Tensile Test			Compression Test				
% R (ϕ_R^0)	T_i (°C)	E (GPa)	σ_R (MPa)	ϵ_R (%)	σ_y (MPa)	ϵ_y (%)	ϕ_R^c (%) (2)	V_D (SEM) (%) (2)	${}_E T_{g\infty}$ (°C) (2)
0		2.4 ± 0.07	53	2.75	128 ± 6	12.3	—	—	176
6.5	50	2.18 ± 0.06	39	2.1	111 ± 6	13.6	2.9	10.7	168
(7.6)	75	2.26 ± 0.07	55	3.7	114 ± 6	13.3	3.1	8.9	167
10.6	50	1.88 ± 0.06	53	3.7	103 ± 5	14.2	4.1	13.2	168
(12.3)	75	1.71 ± 0.05	47	3.3	105 ± 5	14.1	4.3	17.2	162
15	29	1.7 ± 0.05	47	4.2	81 ± 4	11.3	6.1	29.7	155
(17.3)	50	1.83 ± 0.05	53	4.7	85 ± 4	11.4	6.4	25.4	154
	75	1.84 ± 0.05	50	4.0	83 ± 4	11	6.1	24.8	155
	100	1.82 ± 0.05	51	4.3	82 ± 4	11.2	6.6	22.0	153
20 (22.9)	75	1.34 ± 0.04	46	4.9	69 ± 3	12.0	7.1	29.0	151

V_D (SEM): volume fraction of dispersed phase; ϕ_R^c: volume fraction of rubber dissolved in the matrix; ϕ_R^0: initial volume fraction of rubber added to the formulation; % R: initial mass fraction of rubber added to the formulation; T_i: precure temperature.

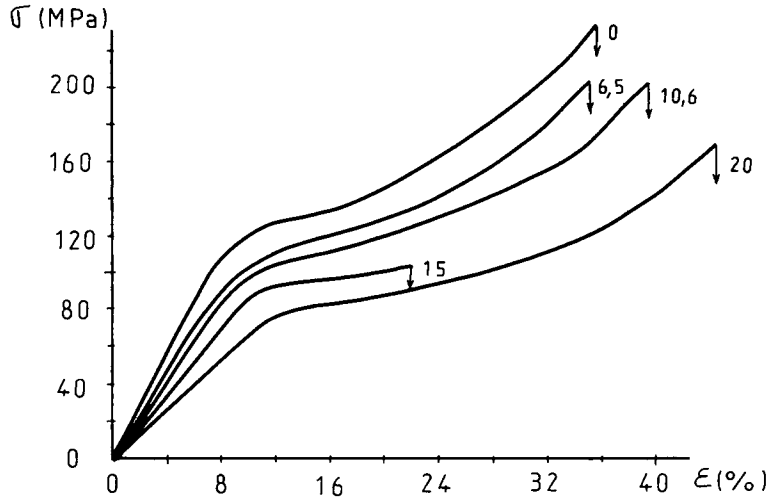

Figure 4 Influence of rubber content on the compressive stress–strain curves of rubber-modified epoxies ($\dot{\epsilon} = 8 \cdot 10^{-4}\ s^{-1}$) at room temperature. Systems: DGEBA ($\bar{n} = 0.03$)–3DCM–n% R8; 6.5% R8; 10.6% R8; 15% R8; 20% R8 cycle 75°C.

with the rubber content[4,7–11,19] and the relative amounts of dissolved and phase-separated rubber increase when the initial rubber content increases (Table I). The slight decrease in the ${}_E T_{g_\infty}$, is due to an increase in the dissolved rubber in the epoxy–amine matrix, as calculated in the second part.[2]

Compression tests at room temperature reveal similar upper-yield stresses related to the shear deformation process for all the samples (Fig. 4 and Table I). The shear yielding process is favored by an increasing rubber content.

We obtain a linear relation between the Young's moduli, E, or the yield stress, σ_y, versus the volume fraction of dispersed phase, V_D (SEM) (Fig. 5).

As found by Brown,[32] the ratio of the yield stress to the Young's modulus, σ_y/E, is nearly constant, and we obtained the value 0.05 for all the systems, even when the amount of R8 rubber changes. However, this value is not in the range determined by Brown for glassy polymers, which is between about 0.017 and 0.03. For thermosetting resins, this ratio seems to be higher.

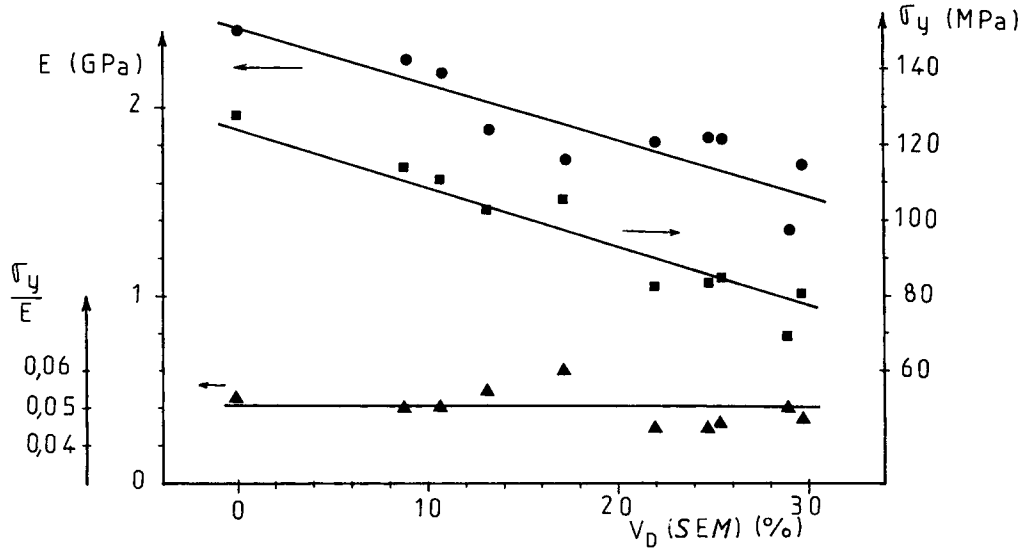

Figure 5 Changes in Young's modulus, E, yield stress, σ_y, and the ratio σ_y/E with the volume fraction of dispersed phase, V_D (SEM). Systems: DGEBA ($\bar{n} = 0.03$)–3DCM–n% R8.

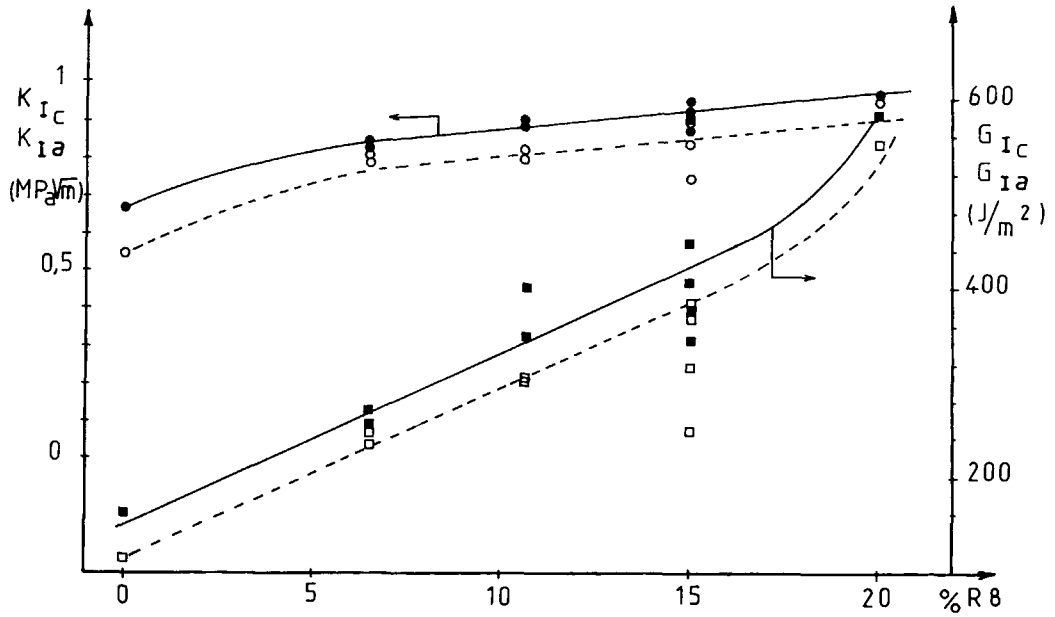

Figure 6 Evolution of K_{Ic} (●), K_{Ia} (○), G_{Ic} (■), G_{Ia} (□) with the initial rubber content. System: DGEBA ($\bar{n}$ = 0.03)–3DCM–n% R8.

Deformation and Fracture Behavior

K_{Ic} was determined by performing a least-squares fit to a plot of σ_c as a function of $[\sqrt{\pi a} \cdot Y(a/w)]^{-1}$.

In this investigation, we consider fracture toughness of the various materials in terms of the critical strain–energy release rate, G_{Ic}, because it takes into account the changes in stiffness.

For our systems and conditions, crack propagation occurs in a stick-slip manner exhibiting load values appropriate to crack initiation and crack arrest. K_{Ic} and K_{Ia} are the stress intensity factors for initiation and arrest, respectively, and the differences between them characterizes the amount of jumping that has taken place. When K_{Ic} is equal to K_{Ia}, propagation is stable. The influence of rubber content on K_{Ic} and K_{Ia} is represented in Table I and Figure 6. When the rubber content increases, K_{Ic}, K_{Ia}, G_{Ic}, and G_{Ia} increase. For example, when the rubber content increases from 0 to 20% R8, K_{Ic}, and G_{Ic} vary from 0.67 MPa · $\sqrt{m}$ to 0.97 MPa · $\sqrt{m}$ and 163 J/m^2 to 588 J/m^2, respectively. When the amount of rubber increases, the stick-slip propagation transforms into a stable propagation.

The toughness of rubber-toughened thermosets increases with the volume fraction of the dispersed rubbery phase, V_D, but the modulus and yield strength usually decrease slightly.[11,14,17,18,29] For our systems, fracture resistance as measured by G_{Ic} increased linearly with the rubber-phase volume (Fig. 7). We confirm the previous work of Bucknall and Yoshii[11] and Yee and Pearson[19–21] who also found a linear relation between G_{Ic} and V_D. Kunz et al.[10] and Kinloch[14] indicate that the dependence of G_{Ic} upon V_D is a function of the test temperature and rate. There is a strong dependency of the fracture energy on the temperature largely arising from the inherent ductility of the matrix that is temperature-dependent. The rubbery particles increase the fracture energy by facilitating a greater extent of energy dissipating deformations in the vicinity of the crack tip.[29] The main deformation process in rubber-modified epoxy networks is shear yielding[6,18] associated with cavitation.[19–21]

We also find a linear relation between K_{Ic} or G_{Ic} and $\bar{D}/\overline{dp}$ (Fig. 8), where $\bar{D}$ is the mean particle diameter and $\overline{dp}$ is the mean interparticle distance. The ratio $\bar{D}/\overline{dp}$ seems, in our case, to be the parameter that takes into account both the influence of V_D and particle size. The overlapping of stress fields seems to be more efficient for $\bar{D}/\overline{dp} > 1$ thus for $V_D \geq 20\%$. For our case, we find a ratio less than 1 except for the cure cycle at 29°C. This low value can explain the small reinforcement with 3DCM. In comparison, Montarnal et al.[8] with DGEBA ($\bar{n}$ = 0.15)–MNDA-15% R8, find a ratio greater than 2 and good toughness; the resilience, Rs, with 15% R8 at 75°C increases by a factor of 3.4 in comparison to a system without rubber.

Plastic shear yielding in the matrix is the main

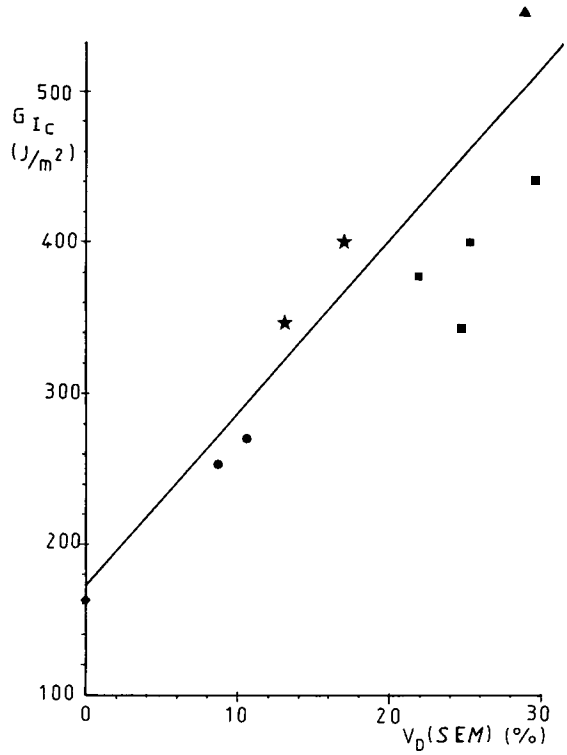

Figure 7 Relationship between G_{Ic} and the volume fraction of dispersed phase. Systems: DGEBA ($\bar{n}$ = 0.03)–3DCM–n% R8 (♦) 0%; (●) 6.5%; (*) 10.6%; (■) 15%; (▲) 20%.

source of energy dissipation and increased toughness. Such plastic deformation occurs to a greater extent in the matrix of rubber-toughened thermosets than in the unmodified material, due to interactions between the stress field ahead of the crack and the rubbery particles.

The ratio $\bar{D}/\overline{dp}$ takes into account the value of V_D by the intermediate of $\overline{dp}$. Wu[33] has analyzed the effects of rubber particle size and rubber–matrix adhesion on notched impact toughness of nylon–rubber blends. Wu found that the blends undergo a sharp tough-brittle transition, when the interparticle distance is at a critical value, and this author supposes that the critical interparticle distance is the only characteristic parameter that determines whether a blend will be tough or brittle.

Goodier[34] has derived equations for the stresses around an isolated elastic spherical particle embedded in an isotropic elastic matrix that is subjected to an applied uniaxial tensile stress far away from the particle. This equation shows that for a rubbery particle, which typically possesses a considerably lower shear modulus than does the matrix, the maximum stress concentration occurs at the equator of the particle and has a value of about 1.8. More recently, Broutman and Panizza[16] have used finite element stress analysis to obtain the stress concentration around rubbery particles for the case when the particle volume fraction is sufficiently high that the particle stress fields interact. Their model indicates that the stress concentration around rubber particles is at maximum at the particle equator and decreases progressively with the distance. Furthermore, assuming the matrix is well bonded to the particle, this stress is a triaxial tension stress.[15]

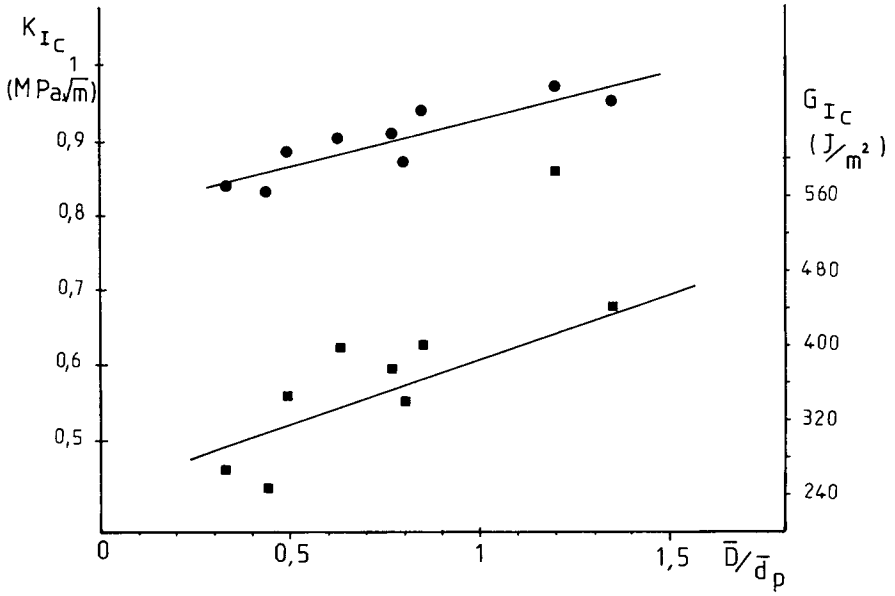

Figure 8 K_{Ic} (●) and G_{Ic} (■) as functions of $\bar{D}/\overline{dp}$. Systems: DGEBA ($\bar{n}$ = 0.03)–3DCM–n% R8.

Table II Mechanical Properties and Morphology as Functions of Cure Schedule for Specimens with Different Percentages of Rubber after SEN Tests ($\dot{\epsilon} = 5.2 \cdot 10^{-4}$ s^{-1}) at Room Temperature

% R8 (ϕ_R^0)	T_i (°C)	K_{Ic} (MPa·$\sqrt{m}$)	K_{Ia} (MPa·$\sqrt{m}$)	G_{Ic} (J/m^2)	G_{Ia} (J/m^2)	$\bar{D}$ (μm) (2)	$\overline{dp}$ (μm) (2)	ϕ_R^c (%) (2)	V_D (SEM) (%) (2)	$\frac{K_{Ic}(n\%)}{K_{Ic}(0\%)}$	$\frac{G_{Ic}(n\%)}{G_{Ic}(0\%)}$
0		0.67	0.55	163 ± 8	110	/	/	0	0	1	1
6.5	50	0.84	0.78	272 ± 14	232	0.26	0.78	2.9	10.7	1.3	1.67
(7.6)	75	0.83	0.82	255 ± 13	245	0.36	0.81	3.1	8.9	1.24	1.56
10.6	50	0.89	0.82	348 ± 17	195	0.31	0.63	4.1	13.2	1.32	2.13
(12.3)	75	0.91	0.79	401 ± 20	305	0.37	0.59	4.3	17.2	1.36	2.46
15	29	0.95	0.89	442 ± 22	388	0.27	0.20	6.1	29.7	1.42	2.71
(17.3)	50	0.94	0.74	402 ± 20	249	0.35	0.41	6.4	25.4	1.4	2.47
	75	0.87	0.84	342 ± 17	319	0.43	0.54	6.1	24.8	1.3	2.1
	100	0.91	0.91	379 ± 19	379	0.46	0.65	6.6	22.0	1.36	2.33
20 (22.9)	75	0.97	0.94	588 ± 29	554	0.55	0.46	7.1	29.0	1.45	3.6

Influence of an Isothermal Precure Schedule on Mechanical Properties

We have detailed the morphologies of 15% R8 systems induced by a precure schedule that froze the nodular structure through vitrification or gelation. The overall mechanical properties are summarized in Tables I and II.

We have already seen in the second publication that increasing the cure temperature leads to an increase in the average size of the dispersed domains and the effective volume fraction of dispersed domains does not depend very much on the cure temperature. We also found that concentration of dispersed-phase particles decreases with an increase in the cure temperature.

The Young's moduli are nearly the same (Table I and Fig. 9) when the mean particle diameter varies from 0.27 to 0.46 μm with practically a constant value for the rubber volume fraction V_D (Table I). The Young's modulus is not dependent on the rubber particle size, as already predicted.[8] For the system at 29°C, the value is slightly lower because V_D is slightly higher for this system (see Table I).

Compression tests at room temperature reveal similar yield stresses (near 80 MPa) when the mean diameter increases from 0.27 to 0.46 μm, with practically the same value for the rubber volume fraction V_D.

Concerning the fracture properties, we performed single-edge-notched tests and unnotched instrumented Charpy impact characterizations.[35] The instrumented impact tests exhibit constant values for 15% R8 for the 29, 50, 75, and 100°C precured samples with a resilience Rs = 18 kJ/m^2. For 0% R8, the resilience is equal to 11 kJ/m^2, thus it decreases by a factor of 1.6, which is small (Fig. 9).

With a sterically hindered amine, 1-8 diamino-*p*-menthane (MNDA),[8] toughened with 15% R8 under the same conditions as for 3DCM, the instrumented impact tests exhibit a maximum for the 75°C precured sample with a resilience of Rs = 46 kJ/m^2, which is an unusually high value for rubber-modified thermosets. The resilience Rs is equal to 23, 32, and

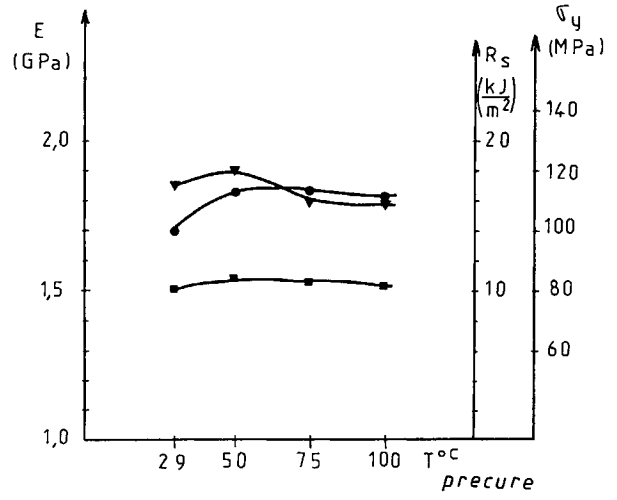

Figure 9 Influence of different curing processes on Young's modulus, yield stress, and resilience. System: DGEBA ($\bar{n}$ = 0.03)–3DCM–15% R8. (●) E; (▼) Rs; (■) σ_y.

28 kJ/m^2 for the 27, 50, and 100°C precured cycles, respectively. The 27°C precured samples are less impact-resistant (23 kJ/m^2) than are the other precure cycles. For this temperature, the mean diameter is 0.53 μm and the volume fraction of the dispersed phase is the same as for the 50, 75, and 100°C precured samples. Montarnal et al.[8] suppose that if the mean diameter is too low (0.5 μm) it is insufficient to enhance the matrix toughening.

With 3DCM and 15% R8, the mean particle diameter, $\bar{D}$, and the ratio $\bar{D}/\overline{dp}$ are less than 0.5 and 1.3 μm, respectively, where $\overline{dp}$ is the mean interparticle distance.

For 15% R8 isothermally cured at different temperatures, 29, 50, 75, and 100°C, the critical stress intensity factor, K_{Ic}, and the fracture energy, G_{Ic}, are practically constant when the mean diameter varies from 0.27 to 0.46 μm for a nearly constant volume fraction of dispersed phase V_D. For the 29°C cycle, V_D is slightly higher and the Young's modulus is slightly lower; as a result, G_{Ic} is higher for this system (Fig. 10 and Table II). Concerning K_a, the difference ΔK ($K_{Ic} - K_{Ia}$) is practically constant when the mean diameter increases from 0.27 to 0.46 μm. At 50°C, ΔK equals 0.2 MPa · $\sqrt{m}$, which is higher than for the other cycles. However, for this system, K_{Ia} was determined with a bad correlation coefficient (0.95), whereas the others are between 0.97 and 0.99. Thus, we can conclude that the cure schedule on 15% R8 influences morphology; however, the values of K_{Ic} and ΔK are nearly the same. In addition, we demonstrated that the mean diameter, which is in the range 0.27–0.46 μm for this system, does not affect the mechanical properties in this case.

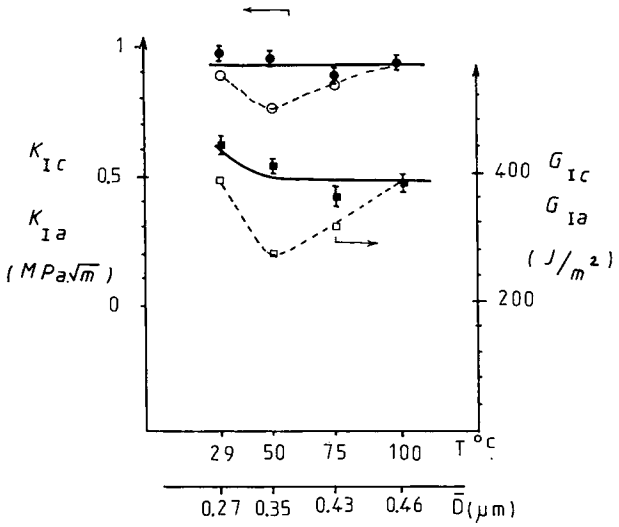

Figure 10 Influence of different curing processes on K_{Ic}, K_{Ia}, G_{Ic}, G_{Ia}, and mean diameter, $\bar{D}$ (μm). System: DGEBA ($\bar{n}$ = 0.03)–3DCM–15% R8.

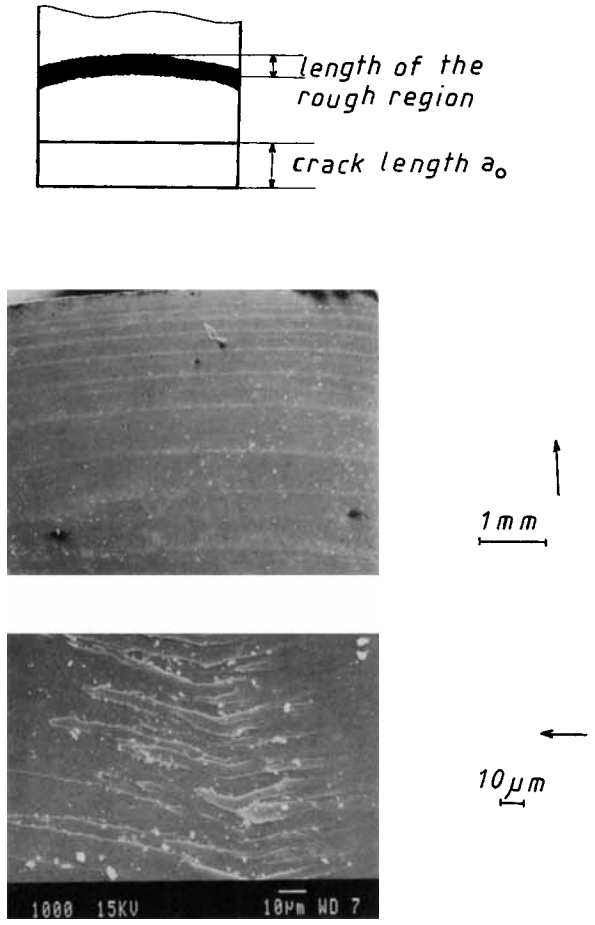

Figure 11 Crack arrest region on fracture surface—specimen fractured in SEN test and observed with SEM.

Toughening by Shear Yielding: Plastic-zone Formation

Bascom et al.[17] found that in rubber-modified epoxies, the plastic-zone size is directly related to the toughness. The stress field associated with the rubbery particles leads to the initiation of two processes that can strongly interact. The first process that occurs is the initiation and growth of shear-yield deformations in the matrix, and the second process is the dilatation and cavitation.[14,19–21] A triaxial stress state usually exists ahead of a crack that produces dilatation and causes failure and void formation either in the particle or at the particle/matrix interface. Cavitation may occur at the rubber particle–matrix interface because of the tensile state from cooling superimposed on the triaxial stress.

The particle cavitation lowers the stress required

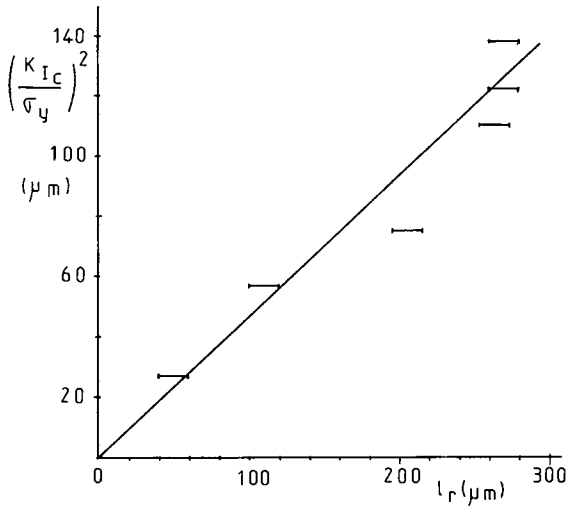

Figure 12 Plot of $(K_{Ic}/\sigma_y)^2$ against the length of the rough-region: L_r, from SEN tests. System: DEGBA ($\bar{n}$ = 0.03)–3DCM–n% R8.

for shear yielding and thus promotes even more extensive plastic shear deformations in the matrix.[14] Yamini and Young[25] have shown that features on the fracture surface at the crack were of the same dimensions as those expected for a Dugdale plastic zone.

We have also shown that the width of the crack arrest line is related to the length of the plastic zone. On the optical micrographs of the crack arrest on the fracture surfaces, we determined the length of the rough region (L_r) (Fig. 11). The length of this feature (L_r) is proportional to the radius of a Dugdale plastic zone, r_p, calculated using the equation $r_p = \pi/8\ (K_{Ic}/\sigma_y)^2$, where σ_y is the yield stress of the material. Figure 12 is a plot of $(K_{Ic}/\sigma_y)^2$ as a function of L_r using the data in Figure 11. During the loading after crack arrest, a plastic zone forms at the tip of the crack. Propagation takes place by slow growth through the plastic zone followed by rapid propagation through the virgin material.

The slow-growth region defines the order of magnitude of the size of the plastic zone at the crack tip, as predicted by Yamini and Young.[25] These authors observed the growth of a crack in an epoxy sample and found that after the "slip" process the crack became stationary at the arrest line and that prior to the next "slip" process it grew slowly through a small region before bursting through and jumping ahead. Yamini and Young[25] found that the length of the slow-growth region, L_r, is closely related to r_p. In our case, we determined the length of the rough region (L_r) that contains the slow-growth region and the beginning of the fast propagation. We determined a slope value of 0.48, which is lower than the value of $8/\pi$ found by Yamini and Young.

Like Hollmann and Hann,[30] we have also seen on the fracture surfaces that when K_{Ic} increases, i.e., when the % R8 increases, the number of "slip" decreases. For the same crack length value, for example, for "a" (crack length) equal to 3.2 mm, the number of slip varies from 6 to 1 or 2 when the % of rubber increases from 0 to 20% R8, and the crack grows stably.

Cavitation and Plastic-zone Formation

Bascom et al.[17] and Yee and Pearson[19–21] proposed that cavitation and plastic shear yielding of the epoxy matrix are the microdeformation mechanisms occurring at the crack tip that dissipate energy and produce the toughening effect.

For seeing the presence of cavitation with 15% R8, we have used tensile creep dilatometry.[36] A constant load equal to 40 MPa was applied, and the volume strain, $\Delta V/V_0$, where ΔV is the change in volume and V_0 is the original volume, and ϵ_L and ϵ_T, the longitudinal and transverse engineering strains, were determined. For the 15% R8 system, isothermally cured at different temperatures (T_c = 29, 50, 75, and 100°C), we always find the same results (Fig. 13). The value of $\Delta V/V_0$ and ϵ_L are less than 0.7% and 4.2%, respectively. For 0% R8, $\Delta V/V_0$ is equal to 0.2% and ϵ_L equals 2.8%. Figure 13 shows the volume dilatation behavior of the neat resin (0% R8) and the 15% R8 resin. The volume dilatation behavior of the rubber-modified epoxies appears to be very similar to those of the neat resin. The form of the curves is similar, but the values of $\Delta V/V_0$ and

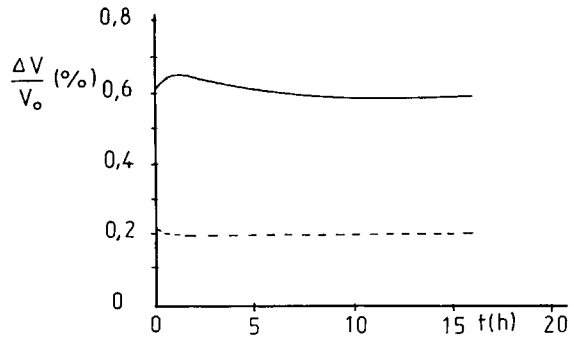

Figure 13 Change in $\Delta V/V_0$ with time in creep measurements: (——) DGEBA–3DCM–15% R8; (-----) DGEBA–3DCM–0% R8. The stress is equal to 40 MPa.

ϵ_L are a little higher with rubber. However, we do not see an increase in $\Delta V/V_0$ or ϵ_L with rubber content like Yee and Pearson[19-21] who found values for $\Delta V/V_0$ and ϵ_L double those that we found. With 3DCM, the tensile dilatometry results indicate that the rubber particles enhance shear flow and slightly promote cavitation. Both mechanisms facilitate the shear localization process and result in enhanced toughness by the formation of a plastic zone ahead of the crack tip. With 3DCM, the second mechanism is not preponderant, which is perhaps due to the diameter of the rubber particles of less than 0.5 μm.

CONCLUSION

Rubber-enhanced shear deformation of the matrix is regarded as the major toughening mechanism. Plastic shear yielding in the matrix is the main source of energy dissipation and increased toughness. Such plastic deformation occurs to a far greater extent in the matrix of rubber-toughened thermosets, compared with the unmodified material, due to interactions between the stress field ahead of the crack and the rubbery particles.

With rubber incorporation, impact strength, fracture toughness (K_{Ic}), and fracture energy (G_{Ic}) were increased, while Young's modulus and yield strength decreased slightly. This slight decrease is due to an increase in the dissolved rubber in the epoxy–amine matrix.

Concerning the relation between morphology and mechanical properties, with 3DCM, the variation of the mean diameter $\bar{D}$ between 0.27 and 0.46 μm for the same volume fraction or the rubber phase has no significant effect on the mechanical properties. The volume fraction of the rubber phase, V_D, is a dominant factor affecting fracture resistance. We obtain a linear relation between G_{Ic} and V_D or $\bar{D}/\overline{dp}$, where $\overline{dp}$ is the mean distance between two particles, surface to surface.

The crack propagation behavior in epoxy resins is controlled by the plastic deformation characteristics of the material. It has been shown that the width of the crack arrest line that is found on the fracture surfaces of specimens undergoing stick-slip behavior is of the same dimensions as that expected for a Dugdale plastic zone. Because of the reduced presence of cavitation with 3DCM, the toughness is not high for the elastomer-modified epoxies systems.

We would like to thank Professor C. B. Bucknall and I. Partridge for the dilatometry creep measurements. This work was performed in the frame of a cooperation program between the National Research Councils of France (CNRS) and Argentina (CONICET).

REFERENCES

1. D. Verchère, H. Sautereau, J. P. Pascault, S. M. Moschiar, C. C. Riccardi, and R. J. J. Williams, *J. Appl. Polym. Sci.*, **41,** 467 (1990).
2. D. Verchère, J. P. Pascault, H. Sautereau, C. C. Riccardi, S. Moschiar, and R. J. J. Williams, *J. Appl. Polym. Sci.*,**42,** 701 (1991).
3. S. M. Moschiar, C. C. Riccardi, R. J. J. Williams, D. Verchere, H. Sautereau, J. P. Pascault, *J. Appl. Polym. Sci.*, **42,** 717 (1991).
4. L. T. Manzione, J. K. Gillham, and C. A. Mc Pherson, *J. Appl. Polym. Sci.*, **26,** 889 (1981).
5. L. T. Manzione, J. K. Gillham, and C. A. Mc Pherson, *J. Appl. Polym. Sci.*, **26,** 907 (1981).
6. L. C. Chan, J. K. Gillham, A. J. Kinloch, and S. J. Shaw, Adv. Chem. Ser. 208, C. K. Riew and J. K. Gillham, Eds., American Chemical Society, Washington, DC, 1984, p. 235.
7. P. Bartlet, J. P. Pascault, and H. Sautereau, *J. Appl. Polym. Sci.*, **30,** 2955 (1985).
8. S. Montarnal, H. Sautereau, and J. P. Pascault, Adv. Chem. Ser. 222, C. K. Riew Ed., American Chemical Society, Washington, DC, 1989, p. 193.
9. S. C. Kunz, J. A. Sayre, and R. A. Assink, *Polymer,* **23,** 1897 (1982).
10. J. F. Hwang, J. A. Manson, R. W. Hertzberg, G. A. Miller, and L. H. Sperling, *Polym. Eng. Sci.*, **29,** 1466 (1989).
11. C. B. Bucknall and P. Yoshii, *Br. Polym. J.*, **10,** 53 (1978).
12. C. K. Riew, Adv. Chem. Ser. 222, C. K. Riew Ed., American Chemical Society, Washington, DC, 1989.
13. A. J. Kinloch and D. L. Hunston, *J. Mater. Sci. Lett.*, **5,** 1207 (1986).
14. A. J. Kinloch, in *Structural Adhesives,* A. J. Kinloch, Ed., Elsevier, London, 1986, p. 127.
15. R. S. Raghava, *J. Appl. Polym. Sci.*, **25,** 1017 (1987).
16. L. T. Broutman and G. Panizza, *Int. J. Polym. Mater.*, **1,** 95 (1971).
17. W. D. Bascom, R. L. Cottington, R. L. Jones, and P. Peyser, *J. Appl. Polym. Sci.*, **19,** 2545 (1975).
18. A. J. Kinloch, S. J. Shaw, and D. L. Hunston, *Polymer,* **24,** 1355 (1983).
19. A. F. Yee and R. A. Pearson, *J. Mater. Sci.*, **21,** 2462 (1986).
20. R. A. Pearson and A. F. Yee, *J. Mater. Sci.*, **21,** 2475 (1986).
21. R. A. Pearson and A. F. Yee, *J. Mater. Sci.*, **24,** 2571 (1989).
22. S. Yamini and R. J. Young, *J. Mater. Sci.*, **15,** 1823 (1980).

23. A. J. Kinloch and J. G. Williams, *J. Mater. Sci.*, **15,** 587 (1980).
24. S. Yamini and R. J. Young, *J. Mater. Sci.*, **14,** 1609 (1979).
25. S. Yamini and R. J. Young, *J. Mater. Sci.*, **15,** 1814 (1980).
26. C. Phillips, J. M. Scott, and M. Jones, *J. Mater. Sci.*, **13,** 311 (1978).
27. J. M. Scott, G. M. Wells, and D. C. Phillips, *J. Mater. Sci.*, **15,** 1436 (1980).
28. S. Hashemi and J. G. Williams, *J. Mater. Sci.*, **19,** 3746 (1984).
29. A. J. Kinloch, S. J. Shaw, D. A. Tod, and D. L. Hunston, *Polymer,* **24,** 1341 (1983).
30. K. Hollmann and H. T. Hann, *Polym. Eng. Sci.*, **29,** 523 (1989).
31. J. G. Williams, *Fracture Mechanics of Polymers,* Ellis Horwood, Chichester, 1984.
32. N. Brown, *Mater. Sci. Eng.*, **8,** 69 (1971).
33. S. Wu, *Polymer,* **26,** 1855 (1985).
34. J. N. Goodier, *Trans. Am. Soc. Mech. Eng.*, **55,** 39 (1933).
35. G. Merle, Y. S. O, C. Pillot, and H. Sautereau, *Polym. Test.*, **5,** 37 (1985).
36. M. W. Darlington and D. W. Saunders, *J. Phys.*, **E3,** 571 (1970).

Received April 16, 1990
Accepted November 27, 1990